PHILOSOPHICAL TRANSACTIONS A

Phil. Trans. R. Soc. A.
doi:10.1098/not yet assigned

Kinetics of thermal-assisted delayed fluorescence in blue organic emitters with large singlet–triplet energy gap

Fernando B. Dias

Department of Physics, University of Durham, DH1 3LE, UK

Keywords: TADF, Delayed Fluorescence, OLEDs, Reverse Intersystem crossing, TTA

The kinetics of thermally activated delayed fluorescence (TADF) is investigated in dilute solutions of organic materials. A new method to accurately determine the energy barrier and the rate of reverse intersystem crossing is developed. This methodology is then applied to blue emitting OLED materials with larger singlet-triplet energy gap. In these materials, TADF is able to compete with triplet-triplet annihilation (TTA) above a threshold temperature; however, TTA is still the dominant mechanism. Strong evidence is obtained for the role of heteroatoms, on the enhancement of reverse intersystem crossing in these materials.

I. INTRODUCTION

Thermal Activated Delayed Fluorescence (TADF) has recently become one of the favorite methods to overcome the 25% limitation on the internal quantum efficiency of organic light emitting devices (OLEDs) due to spin statistics.[1,2] In fact, the ratio (1:3) between singlet and triplet excited states, imposes that only 25% of the charge recombination events in OLEDs will give origin to emissive singlet states, the rest is wasted by other non-radiative processes.[3] This imposes a serious limitation for the application of organic materials in displays and lighting devices.[4]

Different methods have been used when trying to overcome this limitation, including the use of organic phosphors containing Ir(III), Pt (II) or other heavy metals, which can convert dark triplet states into emissive species with 100% efficiency due to the enhanced intersystem crossing that is present in these materials via the heavy atom effect. However, these emitting complexes have to be dispersed in charge transporting matrices, which necessarily demand using hosts with high triplet levels, and obtaining stable long-lifetime deep blue emitting phosphors has been proved difficult. Thus, deep blue, long lifetime phosphorescent OLEDs have not yet been demonstrated.[5] Moreover, heavy metals are not abundant elements in nature, which will cause unnecessary stress on the fabrication costs of these devices.

Using triplet-triplet annihilation (TTA) to up-convert non-emissive triplet states into emissive singlet states has also been attempted. In this case, the yield of singlet emissive states is highly dependent on the relative energy order of the excited singlet and triplet energy levels, and the maximum total singlet yield is limited to 62.5%. OLEDs with TTA contribution as large as 40% have been demonstrated, but the relative merit of this approach is still unsatisfactory.[6,7]

The TADF mechanism uses the thermal energy to assist reverse intersystem crossing and promote the up-conversion of lower triplet states into more energetic emissive singlet states.[8] Therefore the efficiency of the TADF mechanism is controlled by two main parameters, the energy splitting between the singlet and triplet states (ΔE_{ST}), and the efficiency of non-radiative pathways available for the excited singlet and triplet states.[9,10] Minimization of ΔE_{ST} has been achieved by designing materials with strong intramolecular charge transfer (ICT) character that ensures minimal overlap between the HOMO and LUMO orbitals, and thus zero exchange energy. Singlet-triplet states that are separated by less than 0.1 eV have been achieved, and TADF (E-type fluorescence) emission has been observed with high efficiency in such materials.[11, 12]

As heavy metal complexes, TADF emitters also have to be dispersed in host matrixes with relatively higher triplet level, in order to avoid the concentration quenching of fluorescence, and also the quenching of triplet

*Author for correspondence f.m.b.dias@durham.ac.uk.
†Present address: Physics Department, University of Durham, South Road, Durham, DH1 3LE, UK

states due TTA. Often this leads to host-guest interactions, with formation of emissive exciplex states showing extended fluorescence lifetimes, and more complex photophysics has been observed.[13,14]

Significant progress in recent years has been achieved on the design of materials that emit in the green region of the visible spectrum, however TADF blue emitters are still scarce, and also red emitters with strong TADF contribution are in need. TADF is also finding application in other areas, as for example in Bio-imaging applications due to the extended fluorescence lifetime and large Stokes-shift of these materials, which allows filtering the sample auto fluorescence scattering effects, and avoid the use of fluorescent probes based on heavy metals.[15] Further research work is therefore necessary to fully understand the mechanism and the way molecular structure affects TADF efficiency, in order to support the design of new emitters, with strong fluorescence yields and capable of covering the entire visible spectrum. For this objective the determination of fundamental kinetic parameters in a rapid and accurate manner is of paramount importance.

Here, a kinetic method is developed to accurately and in a rapid way determine the energy barrier and the reverse intersystem crossing rate using the kinetic analysis of TADF materials in dilute solution. Evidence is then obtained for the interplay between triplet-triplet annihilation (TTA) and intramolecular thermal assisted reverse intersystem crossing (Risc) in materials with singlet-triplet energy gaps much larger than the kT energy at room temperature.

II. Methods.

Solutions (10^{-5}-10^{-4} M) of all materials were degassed using 5 freeze/thaw cycles. Absorption and emission spectra are collected using a UV-3600 double beam spectrophotometer (Shimadzu), and a Fluorolog fluorescence spectrometer (Jobin Yvon). Temperature dependent measurements were acquired using a model liquid nitrogen cryostat (Janis Research). Phosphorescence, prompt fluorescence (PF) and delayed emissions (DF) spectra and decays were recorded using nanosecond gated luminescence and lifetime measurements (from 400 ps to 1 s) using a high energy pulsed Nd:YAG laser emitting at 355 nm (EKSPLA). Emission was focused onto a spectrograph and detected on a sensitive gated iCCD camera (Stanford Computer Optics) having sub-nanosecond resolution. PF/DF time resolved measurements were performed by exponentially increasing gate and delay times, details can be found elsewhere.[16]

III. Kinetics of TADF.

Figure 1represents the energy diagram describing the kinetics of TADF in the long time regime, i.e. after the prompt component of the fluorescence emission has vanished. Neglecting the prompt fluorescence component in this analysis is entirely justified, since the lifetime of the prompt fluorescence component is much shorter than the delayed fluorescence lifetime. The kinetic equations derived from figure 1, therefore take into account only the singlet excited states that are formed from reverse intersystem crossing, and neglect the decay terms associated with the prompt component.

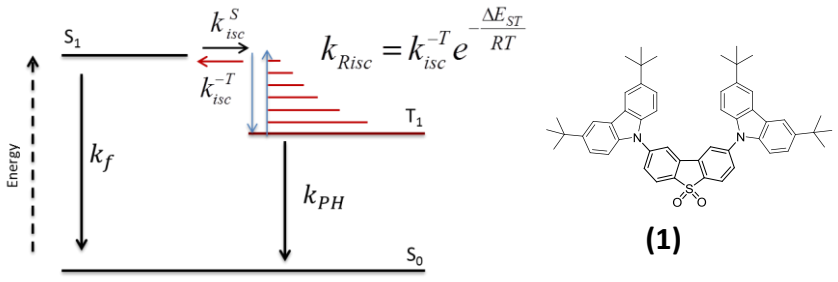

Figure 1-Simplified energy diagram representing the up-conversion of triplet states (T_1) to higher energy singlet states (S_1). k_{Risc} is the reverse intersystem crossing rate from T_1, and k_f, k_{PH}, represent the decay rates of singlet and triplet states to the ground state respectively, including the internal conversion processes. k_{isc}^{S}, and k_{isc}^{-T} are the intersystem crossing rate from T_1, and the maximum reverse intersystem crossing rate, obtained from upper triplet levels to the S_1 manifold. The chemical structure of compound (1) is shown on the right.

The S_1 and T_1 populations are described in the long time range by equations (1) and (2).

$$\frac{dS_1}{dt} = -k_f S_1 + k_{Risc} T_1 \qquad (1)$$

$$\frac{dT_1}{dt} = -(k_{Risc} + k_{PH}) T_1 \qquad (2)$$

Solving (1) and (2) gives:

$$T_1(t) = T_0 e^{-Xt} \qquad (3)$$

$$S_1(t) = \frac{k_{Risc}}{k_f - X} T_0 e^{-Xt} \qquad (4)$$

where $X = k_{Risc} + k_{PH}$. The first observation is that the in the case of TADF, the delayed fluorescence decays with the triplet lifetime as expected. We use equation (4) to determine the steady-state intensity of the delayed emission, given by eq. (5), where k_{f0} represents the natural radiative decay rate constant, and $f_{inst}$is an instrumental factor.

$$I_{TADF}^{SS} = f_{inst} k_{f0} \int_0^{+\infty} S_1(t) dt = f_{inst} k_{f0} \frac{T_0 k_{Risc}}{X(k_f - X)} \qquad (5)$$

Since $k_f \gg X$ eq. (5) can be simplified:

$$I_{TADF}^{SS} = f_{inst} k_{f0} \frac{T_0 k_{Risc}}{X k_f} \qquad (6)$$

From eq. (6) is clear that in the case of TADF, the delayed fluorescence intensity depends linearly with the excitation dose, i.e. in a log/log graph of I_{TADF}^{SS} vs. excitation dose, at constant temperature, the gradient is one. This is in strong contrast with the delayed fluorescence appearing from triplet-triplet annihilation (TTA). In the TTA case, the variation of the steady-state delayed fluorescence intensity with excitation dose, depends on the competition between the rate for triplet monomolecular decay, k_{PH}, and the rate for diffusion collisional quenching of triplets, k_{TTA}. When the former dominates, i.e. the triplets deactivate more quickly than the rate of triplet collisional diffusion ($k_{TTA}[T_1] \ll k_{PH}[T_1]$), the I_{TTA}^{SS} shows a quadratic dependence with the excitation dose (eq. 7), but when TTA dominates, at higher triplet concentration, the I_{TTA}^{SS} dependence with excitation dose turns to a linear regime (eq. 8), where *f* represents the fraction of encounters between two triplets.[17]

$$I_{TTA}^{SS} = \frac{f k_{TTA}}{2 k_{PH}} T_0^2 \qquad (7)$$

$$I_{TTA}^{SS} = \frac{1}{2} f T_0 \qquad (8)$$

Two clear temperature regimes can be defined for TADF from eq. (6). In the high temperature limit (HTL), $k_{Risc} \gg k_{PH}$ and $X \approx k_{Risc}$, thus eq. (6) further simplifies to:

$$I_{TADF}^{SS} = f_{inst} k_{f0} \frac{T_0}{k_f} \qquad (9)$$

In this temperature limit, the intensity of the delayed fluorescence appearing from TADF is temperature independent, providing that T_0, k_{f0}, and k_f are all not significantly affected by temperature in the interval used to follow the TADF. This is easily confirmed by following the intensity and fluorescence lifetime.

In the low temperature limit (LTL), $k_{Risc} \ll k_{PH}$, and $X \approx k_{PH}$, in this regime eq. (6) is simplified to give:

$$I_{TADF}^{SS} = f_{inst} k_{f0} \frac{T_0 k_{Risc}}{k_{PH} k_f} \qquad (10)$$

Using the Arrhenius temperature dependence of the reverse intersystem crossing rate, $k_{Risc} = k_{Risc}^0 e^{-\Delta E_a/RT}$, the energy barrier associated with TADF (ΔE_a), is determined directly from eq. (10). Usually the assumption is that this energy barrier is simply given by the S_1-T_1 energy splitting (ΔE_{ST}), which is simply determined from fluorescence (S_1) and phosphorescence (T_1) spectra. However, fluorescence from TADF emitters is usually broad and void of vibrational structure, due to the strong charge transfer character of the lowest S_1 state, and this makes difficult to determine the energy of S_1 precisely. Moreover, phosphorescence is also usually observed at low temperature, and often the maximum of the phosphorescence emission spectrum shifts with temperature, which introduces another uncertainty on the determination of ΔE_{ST}. Additionally, from measurements of the prompt and delayed fluorescence lifetime, k_{Risc}, is determined, and since (ΔE_a) has been determined independently from (10), the maximum reverse intersystem crossing rate, appearing from upper triplet levels, k_{Risc}^{-T}, is also obtained.

IV. Results and Discussion.

Figure 2 shows a) the absorption, fluorescence and phosphorescence spectra of (**1**) in ethanol dilute solution, and b) the comparison between the steady-state fluorescence, containing contributions from prompt and delayed components ($I_{PF} + I_{TADF}$), and the delayed fluorescence. Both spectra are in excellent agreement with each other, showing that prompt and delayed fluorescence are originated from the same singlet excited state.

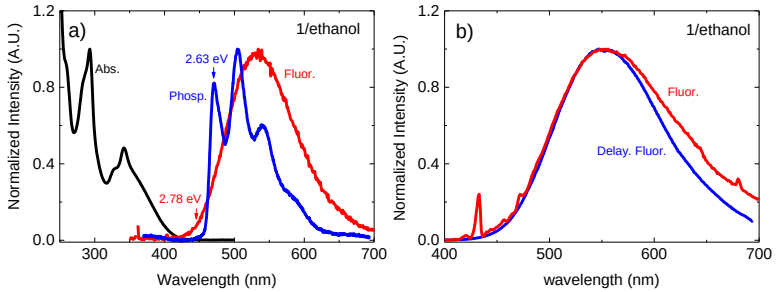

Figure 2- Absorption, fluorescence and phosphorescence spectra of (**1**) in ethanol dilute solution, and b) comparison between the steady-state fluorescence, containing contributions from prompt and delayed components ($I_{PF} + I_{TADF}$), and the delayed fluorescence.

From fig 2a, the energy splitting between singlet and triplet states is estimated as 0.15 eV. Note that the error on this value can be large because of the uncertainty on the S_1 energy, due to the slow rising of the fluorescence onset. Previously we have determined relatively larger S_1-T_1 energy gap for this material using a different approach.[8]

On figure 3a) the fluorescence decay of (**1**), followed over a time interval spanning nine orders of magnitude, shows a clear bi-exponential decay with a fast component of 4.8±0.1ns, assigned to the prompt fluorescence component, and a longer decay of 230±5µs. From fig 3a) the reverse intersystem crossing rate constant is determined using eq. 11, [9,10] $k_{Risc} = (1.9 \pm 0.2) \times 10^2 s^{-1}$.

$$k_{Risc} = \frac{\int I_{TADF}(t)dt}{\int I_{PF}(t)dt} \frac{1}{\tau_{TADF}} \qquad (11)$$

On figure 3b) the variation of the steady-state delayed fluorescence I_{TADF}^{SS} at RT is plotted in a log/log scale against the excitation dose, showing a clear gradient 1, in agreement with eq. 6 for a TADF mechanism.

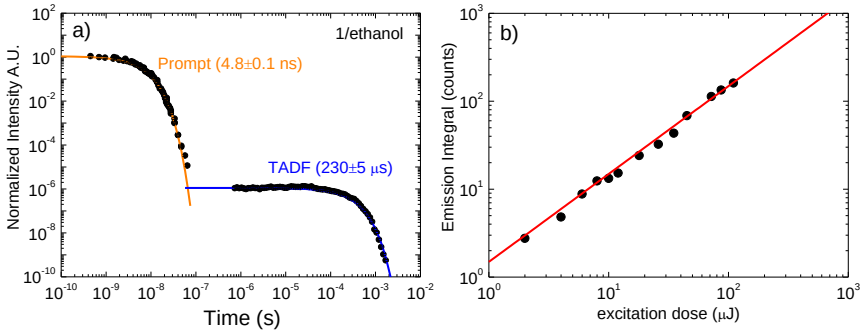

Figure 3-a) Time resolved fluorescence decay of (**1**) in ethanol dilute solution, and b) variation of the steady-state delayed fluorescence with excitation dose, showing that the delayed fluorescence is due to TADF.

The temperature dependence of the delayed fluorescence of (**1**) in ethanol is shown in Figure 4a). Clearly the delayed fluorescence increases with temperature as expected for the TADF mechanism. The plot in figure 4b) shows the HTL and LTL regimes, according with eq. 9 and 10, and from the LTL regime the energy barrier for TADF is determined as ΔEa=0.28±0.02 eV.

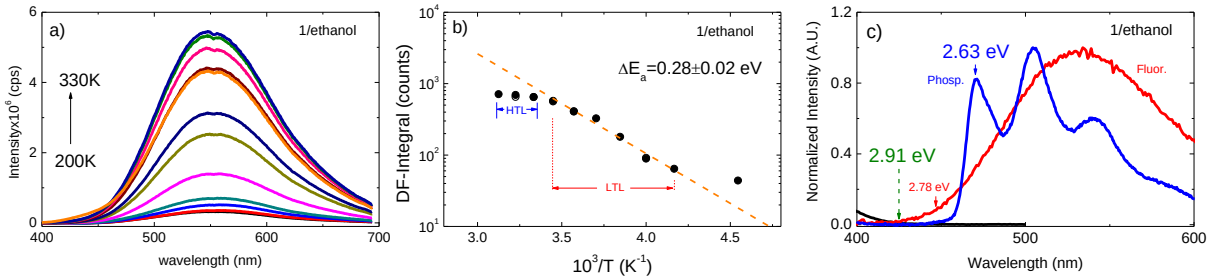

Figure 4-a) Temperature dependence of the steady-state delayed fluorescence of (**1**) in ethanol dilute solution. b) Variation of the delayed fluorescence integral with the reciprocal of temperature, according with equations 9 and 10, and determination of the energy barrier for the TADF. c) Fluorescence and phosphorescence spectra of (**1**) with the S_1 energy corrected for 2.91 eV, 0.28 eV above the T_1 energy.

After determining the energy barrier for TADF, ΔEa=0.28±0.02 eV, and knowing the reverse intersystem crossing rate constant k_{Risc}=(1.9±0.2)x10^2 s^{-1}, the maximum reverse intersystem crossing rate constant $k_{Risc}^{-T} = (1.4 \pm 0.2) \times 10^7 s^{-1}$is also determined. Note that this method of analysis doesn't rely on any complex fittings. On figure 4c) the corrected S_1 energy is highlighted, E_{S1}=2.91±0.02 eV.

Next we move to investigate the delayed fluorescence mechanism in materials with larger singlet-triplet energy gap. These materials are required for emission in the blue region, where the TADF materials formed by relatively strong electron donor-electron acceptor units are more difficult to work, due to the large Stokes-shift induced by the excited state charge transfer.[18] In fact most TADF materials emit in the green region.[19]

Figure 5a), shows the chemical structure of material (2), one of the blue emitters used in this work. Material (2) is a pure non charge transfer material, and only the $^3\pi\pi^*$ and the $^1\pi\pi^*$ transitions are involved on the population of the S_1 excited state. The singlet-triplet energy gap in (2) is large, around 1.1 eV, and therefore TADF is not efficient. Instead the delayed fluorescence appears entirely from TTA.

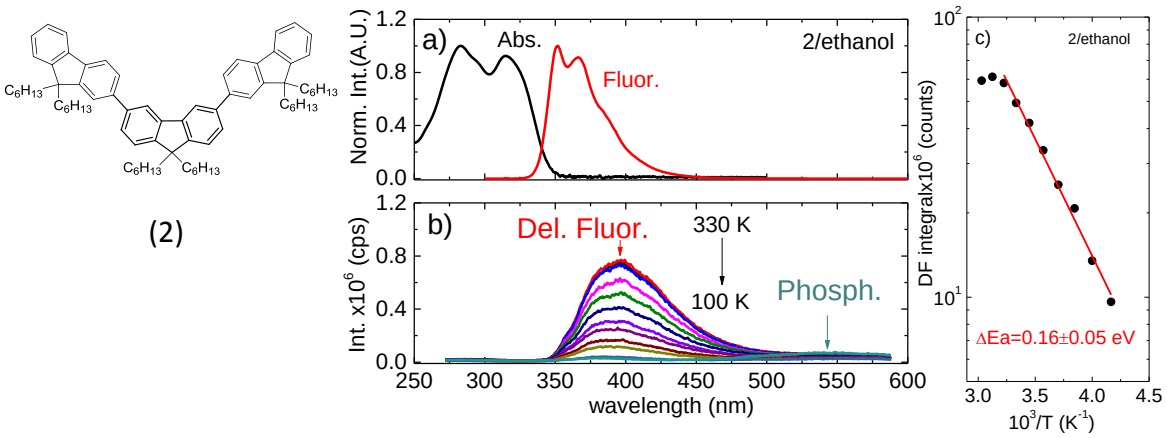

Figure 5- Molecular structure of material (2). a) Absorption and Emission spectra of (2) in ethanol dilute solution. b) Delayed fluorescence obtained in (2) as a function of temperature, weak phosphorescence is observed around 550 nm. c) Temperature dependence of the delayed fluorescence, showing a clear TTA mechanism.

The delayed fluorescence in (2) varies with the square of the excitation dose in agreement with eq. 7, showing that in dilute solutions the monomolecular decay of the triplet state dominates over the triplet collisional diffusion, which originates the delayed fluorescence. A smooth variation of the delayed fluorescence intensity is observed (fig. 5c). The TTA in this regime is controlled by the rate of triplet collisional quenching, and thus by the smooth variation of the solvent viscosity with temperature, and therefore no "turn on" temperature is detected, above which the delayed fluorescence intensity suddenly increases, as it is observed for TADF. Moreover, the energy barrier determined by following the temperature dependence of the delayed fluorescence is 0.16±0.02 eV in excellent agreement with the energy barrier for viscous flow in ethanol (0.15 eV),[20] clearly showing that the origin of the delayed fluorescence is TTA.

Interestingly, in (2) the delayed fluorescence spectrum doesn't entirely match the steady-state fluorescence (fig. 5a & 5b). We assign this behaviour to the effect of changing the nuclear coordinates over time, i.e. the delayed fluorescence appears from molecules having different nuclear configuration from the Franck-Condon (FC) emitters that dominates the prompt fluorescence. This effect is less predominant in TADF materials, because these already emit from non FC states due to their strong ICT nature.

Figure 6 shows the molecular structure of material (3) and (4) with their absorption and fluorescence spectra in hexane and ethanol dilute solution. Both materials have no strong ICT character, confirmed by the lack of a large Stoke-shift, when comparing emissions in non-polar and polar solvents (fig. 6).

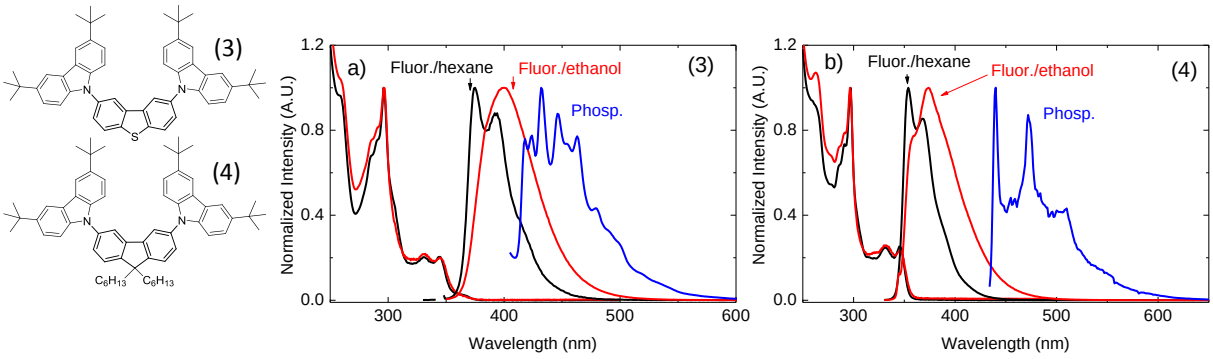

Figure 6- Molecular structures of materials (3) and (4). a) Absorption, fluorescence and phosphorescence of (3) in hexane and ethanol. b) Absorption, fluorescence and phosphorescence of (4) in hexane and ethanol. The phosphorescence is obtained in ethanol at 100K.

The singlet and triplet energy gaps of (3) and (4) are determined from fluorescence and phosphorescence spectra with good precision, $\Delta E_{ST}(3)$=0.47±0.05 eV, and $\Delta E_{ST}(4)$=0.81±0.05 eV. In these materials the emission

raises steeply at the fluorescence spectra onset, due to the weak CT character of the S_1 state, and no major uncertainty on the S_1 energy exists. As expected, due to the non-CT character of (3) and (4) the singlet-triplet energy gaps are significantly larger than in the case of material (1). Therefore the delayed fluorescence from (3) and (4) should appear exclusively from TTA, and the temperature dependence should be similar to that observed for (2), i.e. no contribution from TADF should be observed. Clearly, looking at figure 7, this is not the case.

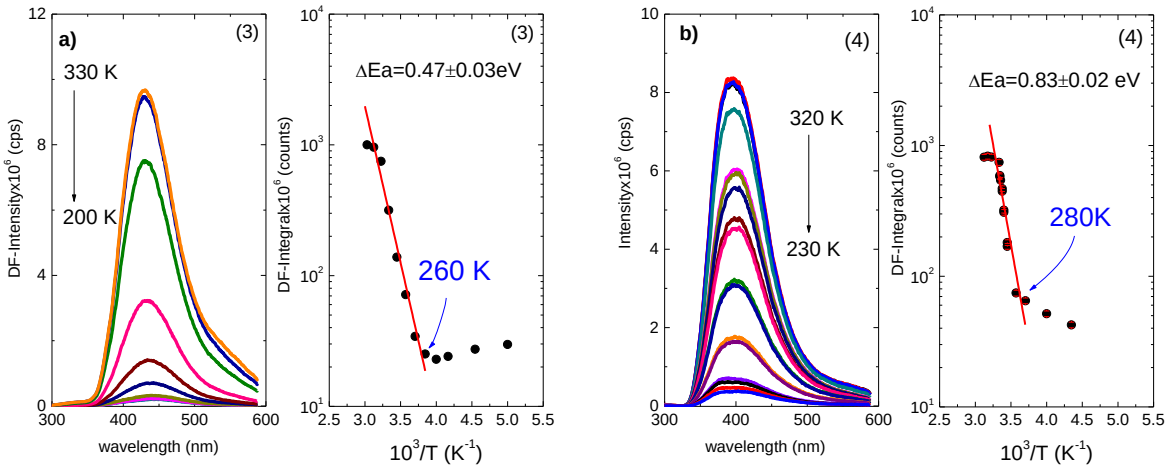

Figure 7- Temperature dependence of the steady-state delayed fluorescence of (3) a), and (4) b), in ethanol dilute solution. The variation of the delayed fluorescence integral with the reciprocal of temperature, according with equations 9 and 10, and determination of the energy barrier for TADF is also shown for each material.

Figure 7 shows the temperature dependence of the delayed fluorescence for materials (3) and (4). Instead of the expected smooth TTA-type temperature dependence, observed with material (2), both materials (3) and (4), show a threshold temperature above which a TADF component is clearly observed. This threshold temperature scales with the magnitude of the singlet-triplet energy gap, moreover, the singlet-triplet energy gap determined from the temperature dependence of the delayed fluorescence, according with eq. 10, agrees exactly with the energy gap determined from the fluorescence/phosphorescence spectra, in clear contrast with material (2). Intriguing, the delayed fluorescence in both materials shows a quadratic dependence with the excitation dose, which indicates TTA is the dominant mechanism that originates the delayed fluorescence.

For TADF to occur the excited triplet levels have to be populated, from which reverse intersystem crossing occurs back to the singlet manifold.[21] In materials with small singlet-triplet energy gap, as material (1), upper triplet levels are populated by the thermal energy bath, and the delayed fluorescence varies linearly with the excitation dose. However, if the singlet-triplet energy gap is large, as it is in (2), and the coupling for reverse intersystem crossing from upper triplet levels is small, the delayed fluorescence can only be obtained via the pure TTA mechanism, and in this case the delayed fluorescence intensity varies in a quadratic manner with the excitation dose.

The behaviour observed in materials (3) and (4), shows that there is an intermediate situation where a mixed mechanism is operative. In this case, TTA is the dominant mechanism for the observation of delayed fluorescence, but above a threshold temperature, which varies with the magnitude of the singlet-triplet energy gap, there is a TADF component that is observed in a relative efficient manner, and despite the large energy gap between the singlet and triplet states is able to compete with TTA. The reason why this mechanism is active is still somehow unclear, but the results strongly indicate that the presence of heteroatoms in the structure of (3) and (4), facilitates the intersystem crossing and the reverse intersystem crossing in these molecules. Note that both (3) and (4) show strong phosphorescence at low temperatures, which can be detected in a simple fluorimeter and using steady-state conditions, i.e. at low temperature phosphorescence is able to compete with fluorescence. In material (2) however, without heteroatoms no contribution from TADF is observed, even at high temperatures, and the phosphorescence is extremely weak at low temperatures. This observations, therefore suggests that heteroatoms facilitate the coupling between the singlet and triplet states in (3) and (4) and are also responsible for the observation of TADF.

V. Conclusions.

In summary, the kinetics of TADF is followed in materials with increasing singlet-triplet energy gap, using a new method that allows to accurately determining the energy barrier and the rate of reverse intersystem crossing, even in molecular materials with strong charge transfer character, where there is a strong uncertainty on the determination of S1 energies.
In materials containing heteroatoms in their structure, the reverse intersystem crossing is facilitated and TADF is observed to compete with TTA in materials with significantly large singlet-triplet energy gap.

Additional Information

Acknowledgments
We thanks Prof Martin Bryce, for kindly providing the materials used in this work.

Data Accessibility
The datasets supporting this article have been uploaded as part of the Supplementary Material.

Competing Interests
I have no competing interests.

References

1. Im, Y., Yeob, J. 2014. Above 20% External Quantum Efficiency in Thermally Activated Delayed Fluorescence Device Using Furodipyridine-Type Host Materials. *Chem. Mater.*, **26**, 1413–1419.

2. Uoyama, H., Goushi, K., Shizu, K., Nomura, H., Adachi, C. 2012. Highly efficient organic light-emitting diodes from delayed fluorescence. *Nature 492,* 234-238. (10.1038/nature11687)

3. Baldo, M. A., O'Brien, D. F., You, Y., Shoustikov, A., Sibley, S., Thompson, M. E., Forrest, S. R. 1998. Highly efficient phosphorescent emission from organic electroluminescent devices. *Nature* **395**, 151-154.

4. Forrest, S. R. 2004. The path to ubiquitous and low-cost organic electronic appliances on plastic. *Nature* **428**, 911-918.

5. Baldo, M. A., Forrest, S. R., Thompson, M. E. 2005. Organic electrophosphorescence, in *Organic Electroluminescence* (Ed: Z. H. Kafafi) CRC press, Taylor & Francis Group, Boca Raton.

6. Kondakov, D. Y., Pawlik, T. D., Hatwar, T. K., Spindler, J. P. 2009. Triplet annihilation exceeding spin statistical limit in highly efficient fluorescent organic light-emitting diodes. *J. Appl. Phys.* **106**, 124510.

7. King, S. M., Cass, M., Pintani, M., Coward, C., Dias, F. B., Monkman, A. P., Roberts, M. 2011. The contribution of triplet-triplet annihilation to the lifetime and efficiency of fluorescent polymer organic light emitting diodes. *J. Appl. Phys.* ***109***, 074502.

8. Dias, F.B., Bourdakos, K.N., Jankus, V., Moss, K.C., Kamtekar, K.T., Bhalla, V., Santos, J., Bryce, M.R., Monkman, A.P. 2013. Triplet Harvesting with 100% Efficiency by Way of Thermally Activated Delayed Fluorescence in Charge Transfer OLED Emitters. *Adv. Mater.* ***25***, 3707–3714.

9. Berberan-Santos, M.N., Garcia, J.M.M. 1996. Unusually strong delayed fluorescence of C70. *J. Am. Chem. Soc.* **118**, 9391-9394.

10. Baleizão, C., Berberan-Santos, M. N. 2007. Thermally activated delayed fluorescence as a cycling process between excited singlet and triplet states: Application to the fullerenes. *J. Chem. Phys.* **126**, 204510.

11. Wu, S., Aonuma, M., Zhang, Q., Huang, S., Nakagawa, T., Kuwabara, K., Adachi, C. 2014. High-efficiency deep-blue organic light-emitting diodes based on a thermally activated delayed fluorescence emitter. *J. Mater. Chem. C*, **2**, 421-424. (10.1039/c3tc31936a).

12. Wang, H., Xie, L., Peng, Q., Meng, L., Wang, Y., Yi, Y., Wang, P. 2014. Novel Thermally Activated Delayed Fluorescence Materials–Thioxanthone Derivatives and Their Applications for Highly Efficient OLEDs. *Adv. Mater.*, *26*, 5198–5204.

13. Jankus, V., Data, P., Graves,D., McGuinness, C., Santos, J., Bryce, M.R., Dias, F.B., Monkman, A.P. 2014. Highly Efficient TADF OLEDs: How the Emitter–Host Interaction Controls Both the Excited State Species and Electrical Properties of the Devices to Achieve Near 100% Triplet Harvesting and High Efficiency. *Adv. Funct. Mater.,* **24**,6178–6186.

14. Méhes, G., Goushi, K., Potscavage Jr., W.J., Adachi, C. 2014. Influence of host matrix on thermally-activated delayed fluorescence: Effects on emission lifetime, photoluminescence quantum yield, and device performance. *Organic Electronics* **15**, 2027–2037.

15. Xiong, X., Song, F., Wang, J., Zhang, Y., Xue, Y., Sun, L., Jiang, N., Gao, P., Tian, L., Peng, X. 2014. Thermally Activated Delayed Fluorescence of Fluorescein Derivative for Time-Resolved and Confocal Fluorescence Imaging. *J. Am. Chem. Soc.*, **136**, 9590–9597.

16. Rothe, C., Monkman, A.P. 2003. Triplet exciton migration in a conjugated polyfluorene *Phys. Rev. B*, **68**, 075208.

17. Hertel, D., Bassler, H., Guentner, R., Scherf, U. 2001. Triplet-triplet annihilation in a polyfluorene-derivative. J. Chem. Phys., **115**, 10007-10013.

18. Dias, F. B., Pollock, S., Hedley, G., Pålsson, L., Monkman, A., Perepichka, I.I.,

Perepichka,I. F., Tavasli, M., Bryce. M.R. 2006. Intramolecular Charge Transfer Assisted by Conformational Changes in the Excited State of Fluorene-dibenzothiophene-*S,S*-dioxide Co-oligomers. *J. Phys. Chem. B*, **110**, 19329-1933.

19. Tao, Y., Yuan, K., Chen, T., Xu, P., Li, H., Chen, R., Zheng, C., Zhang, L., Huang, W. 2014. Thermally Activated Delayed Fluorescence Materials Towards the Breakthrough of Organoelectronics. *Adv. Mater. (*10.1002/adma.201402532*)*

20. Das, K., Ashby, K. D., Wen, J., Petrich, J. W. 1999. Temperature Dependence of the Excited-State Intramolecular Proton Transfer Reaction in Hypericin and Hypocrellin A. *J. Phys. Chem. B*, **103**, 1581-1585.

21. Parker, C. A. 1968. *Photoluminescence of Solutions*, Elsevier Publishing Company, Amesterdam

Figure and table captions

Figure 1-Simplified energy diagram representing the up-conversion of triplet states (T_1) to higher energy singlet states (S_1). k_{Risc} is the reverse intersystem crossing rate from T_1, and k_f, k_{PH}, represent the decay rates of singlet and triplet states to the ground state respectively, including the internal conversion processes. k_{isc}^{S}, and k_{isc}^{-T} are the intersystem crossing rate from T1, and the maximum reverse intersystem crossing rate, obtained from upper triplet levels to the S_1 manifold. The chemical structure of compound (1) is shown on the right.

Figure 2- Absorption, fluorescence and phosphorescence spectra of (**1**) in ethanol dilute solution, and b) comparison between the steady-state fluorescence, containing contributions from prompt and delayed components ($I_{PF} + I_{TADF}$), and the delayed fluorescence.

Figure 3-a) Time resolved fluorescence decay of (**1**) in ethanol dilute solution, and b) variation of the steady-state delayed fluorescence with excitation dose, showing that the delayed fluorescence is TADF.

Figure 4-a) Temperature dependence of the steady-state delayed fluorescence of (**1**) in ethanol dilute solution. b) Variation of the delayed fluorescence integral with the reciprocal of temperature, according with equations 9 and 10, and determination of the energy barrier for the TADF. c) fluorescence and phosphorescence spectra of (1) with the S_1 energy corrected for 2.91 eV, 0.28 eV above the T_1 energy.

Figure 5- Molecular structure of material (2). a) Absorption and Emission spectra of (2) in ethanol dilute solution. b) Delayed fluorescence obtained in (2) as a function of temperature, weak phosphorescence is observed around 550 nm. c) Temperature dependence of the delayed fluorescence, showing a clear TTA mechanism.

Figure 6- Molecular structures of materials (3) and (4). a) Absorption, fluorescence and phosphorescence of (3) in hexane and ethanol. b) Absorption, fluorescence and phosphorescence of (4) in hexane and ethanol. The phosphorescence is obtained in ethanol at 100K.

Figure 7- Temperature dependence of the steady-state delayed fluorescence of (3) a), and (4) b), in ethanol dilute solution. The variation of the delayed fluorescence integral with the reciprocal of temperature, according with equations 9 and 10, and determination of the energy barrier for TADF is also shown for each material.

Figures

For final submissions, figures should be uploaded as separate, high resolution, figure files.

Supplementary material

Supplementary material can be used for supporting data sets, movies, figures and tables, and any other supporting material. The main article, however, should stand on its own merit. Where possible, supplementary material should be combined into one Word document or PDF. A template is available here.